Calculating the thermodynamic properties of planar and spherical liquid-vapour interface

1994 J. Phys.: Condens. Matter 6 6965

(http://iopscience.iop.org/0953-8984/6/35/007)

J. Phys.: Condens. Matter 6 (1994) 6965–6976. Printed in the UK

Calculating the thermodynamic properties of planar and spherical liquid–vapour interface

S M Osman†

Department of Physics, College of Science, Sultan Qaboos University, PO Box 36 Al-Khod Postal Code 123, Muscat, Sultanate of Oman

Received 28 January 1994, in final form 20 June 1994

Abstract. We present results of calculations of the equilibrium density profile and related surface properties for liquid–vapour interface of simple fluids. The interface has been considered to be (i) planar and (ii) spherical, with some attention paid to the stability of small liquid droplets. These calculations are based on density functional theory, in particular the gradient approximation, in conjunction with the simplified random phase approximation Bhatia–Young model for the bulk liquid.

1. Introduction

The simplest semiphenomenological theory of the structure and thermodynamics of the liquid–vapour interface is that due to Van der Waals [1]. In this theory, it is assumed that the Helmholtz free energy is a functional of the density, which can be approximated by a 'local density' contribution plus a term that is proportional to the square gradient of the density, i.e.

$$f[\rho] = \int \mathrm{d}^3 r\, f\big(\rho(r)\big) \tag{1}$$

with

$$f\big(\rho(r)\big) = f_0\big(\rho(r)\big) + \rho(r) v_{\mathrm{ext}}(r) + f_2\big(\rho(r)\big)\big(\nabla\rho(r)\big)^2$$

where the second term, $v_{\mathrm{ext}}(r)$, represents the contribution from any external potential (in our model, the gravitational potential). The term $f_0\big(\rho(\mathrm{v})\big)$ is the free energy density of the uniform liquid and $f_2\big(\rho(r)\big)$ is a positive coefficient that is allowed to vary with temperature.

The approach we follow to determine $f_2\big(\rho(r)\big)$ was first introduced by Yang and co-workers (YFG theory) [2]. This theory relates the coefficient $f_2\big(\rho(r)\big)$ to a microscopic quantity, the second moment of the direct correlation function (DCF), $C(r)$, of the uniform fluid:

$$f_2\big(\rho(r)\big) = \frac{k_{\mathrm{B}}T}{12} \int \mathrm{d}^3 r\, r^2 C(r) \tag{2}$$

where k_{B} and T denote the Boltzmann constant and the absolute temperature, respectively.

† Associate member of The International Centre for Theoretical Physics, Trieste, Italy.

0953-8984/94/356965+12$19.50

Following YFG theory, the grand potential functional, $\Omega[\rho]$, can be obtained as a Legendre transform of $F[\rho]$ using the chemical potential μ, i.e.

$$\Omega[\rho] = F[\rho] - \bar{\mu} \int d^3r\, \rho(r). \tag{3}$$

In order to stabilize the system, $\Omega[\rho]$ has to be minimized subject to the constraint that the total number of molecules $\bar{N}$ is kept constant:

$$\int d^3r\, \rho(r) = \bar{N}. \tag{4}$$

The minimization of the integral in (3) subject to the constraint in (4) leads to an Euler–Lagrange-type equation:

$$2f_2\big(\rho(r)\big)\nabla^2\rho(r) + f_2^1\big(\rho(r)\big)\big(\nabla\rho(r)\big)^2 - f_0^1\big(\rho(r)\big) + \bar{\mu} - v_{\text{ext}}(r) = 0 \tag{5}$$

where

$$f_0^1(\rho) = df_0(\rho)/d\rho \qquad f_2^1(\rho) = df_2(\rho)/d\rho.$$

The solution of (5) for prescribed boundary conditions gives the equilibrium density profile, $\rho(r)$, in the interfacial region.

The surface tension γ follows immediately [2]:

$$\gamma = 2\int_{-\infty}^{\infty} dr\, f_2\big(\rho(r)\big)[\nabla\rho(r)]^2. \tag{6}$$

The YFG theory has been reformulated in an extensive review by Evans [3]. Several authors have applied the theory for a planar liquid–vapour interface, for a single-component liquid [4–6] and binary mixtures [7–9]. To our knowledge, there have been no calculations for a spherical interface. During the last two decades, there have been several attempts to simulate the planar interface by both Monte Carlo [10–12] and molecular dynamics [12] approaches, but only one computer simulation study for liquid droplets [13].

In next section we write down the outlines of our model for the bulk liquid with emphasis on the Bhatia–Young [14] approximation. In section 3 we explain the numerical calculations for solving (5) for both planar and spherical interfaces. In section 4 we present our results. We present our conclusions in section 5.

2. Model for the bulk liquid

We consider a system of particles interacting via a Lennard-Jones (LJ) 12–6 pair potential, characterized by a hard-sphere diameter σ and well depth ϵ:

$$V_{\text{LJ}}(r) = 4\epsilon\left[\left(\frac{\sigma}{r}\right)^{12} - \left(\frac{\sigma}{r}\right)^{6}\right] \tag{7}$$

which can be split into reference potential, $V_{\text{ref}}(r)$, and attractive tail, $V_{\text{tail}}(r)$, contributions. Thus we adopt the following splitting:

$$V_{\text{ref}}(r) = \begin{cases} V_{\text{LJ}}(r) & r < \sigma \\ 0 & r \geqslant \sigma \end{cases}$$

$$V_{\text{tail}}(r) = \begin{cases} 0 & r \leqslant \sigma \\ V_{\text{LJ}}(r) & r > \sigma. \end{cases}$$

For simplicity, we have considered σ to be a temperature- and density-independent parameter. This makes the numerical solution of (5) much less time consuming.

The free energy of the repulsive reference system characterized by the potential $V_{\text{ref}}(r)$ can be replaced with that of an equivalent system of hard spheres (HS) with diameter σ. The bulk properties of the hard-sphere reference system are those obtained from the solution of the familiar Percus–Yevick approximation [15, 16] in conjunction with the compressibility equation of state.

Finally, the Helmholtz free energy density $f_0(\rho)$, pressure $P(\rho)$ and chemical potential $\mu(\rho)$ for the bulk liquid are given within the mean field approximation [4, 5, 14], respectively, by

$$f_0(\rho) = f_{\text{HS}}(\rho) + \tfrac{1}{2}\tilde{V}_{\text{tail}}(0) \tag{8}$$

$$P(\rho) = P_{\text{HS}}(\rho) + \tfrac{1}{2}\rho\tilde{V}_{\text{tail}}(0) \tag{9}$$

$$\mu(\rho) = \mu_{\text{HS}}(\rho) + \tilde{V}_{\text{tail}}(0) \tag{10}$$

where $\tilde{V}_{\text{tail}}(0)$ represents the long-wavelength limit of the Fourier transformation of $V_{\text{tail}}(r)$:

$$\tilde{V}_{\text{tail}}(q) = \rho\int_{\sigma}^{\infty} V_{\text{tail}}(r)ac\sin qrqr4\pi r^2\,\mathrm{d}r. \tag{11}$$

Within the random phase approximation (RPA) [14] we may write the Ornstein–Zernike direct correlation function, $C(r)$, as

$$C(r) = C_{\text{HS}}(r) - \frac{1}{k_{\text{B}}T}\tilde{V}_{\text{tail}}(r). \tag{12}$$

Equations (8), (9) and (10) form a closed set of equations which determine, explicitly, the phase diagram of the bulk phases; while (12) for $C(r)$ is needed for the surface properties determined by the solution of (5).

3. Numerical calculations

For comparison, we have carried out the numerical solutions of (5) for two different interfacial geometries.

3.1. Planar interface

Assuming the fluid possesses a planar interface parallel to the x–y plane, equation (5), in the absence of an external potential, reduces to

$$2f_2(\rho)\frac{\mathrm{d}^2\rho(z)}{\mathrm{d}z^2} + f_2^1(\rho)\left(\frac{\mathrm{d}\rho(z)}{\mathrm{d}z}\right)^2 - f_0^1(\rho) + \bar{\mu} = 0 \tag{5a}$$

whose solution gives the equilibrium density profile $\rho(z)$ providing the boundary conditions

$$\rho(0) = \rho_L \qquad \rho(\infty) = \rho_v. \tag{13}$$

However, the z axis is assumed to be normal to the interface; its origin is arbitrary. We considered $z = 0$ to be somewhere in the bulk liquid .

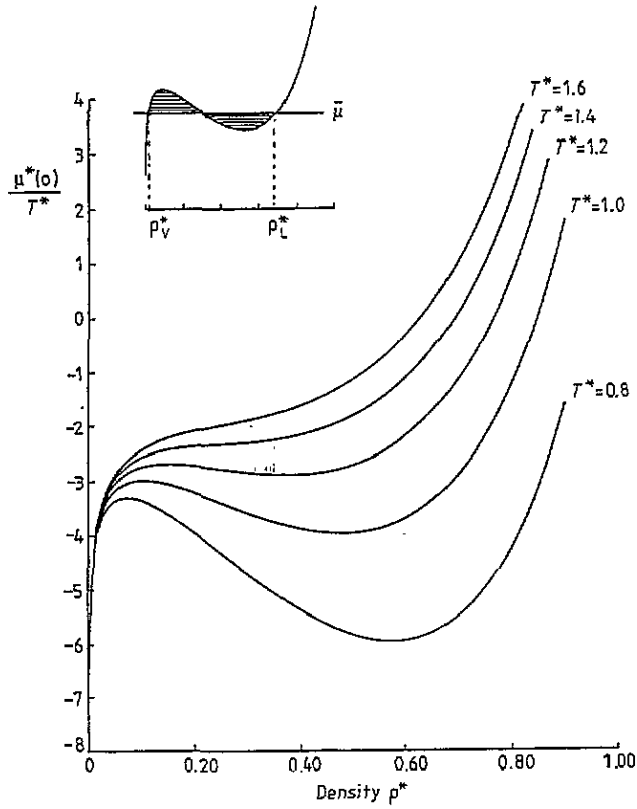

Figure 1. The reduced chemical potential $\mu^*(\rho)$ against reduced density ρ^* at different isotherms together with a schematic diagram for the Maxwell equal-area construction, which is applied only in the case of a planar interface.

The coexistence bulk densities, ρ_L and ρ_u, satisfy the mechanical and chemical equilibrium conditions, namely

$$P(\rho_L) = P(\rho_v) = \bar{P} \qquad \mu(\rho_L) = \mu(\rho_v) = \bar{\mu} \tag{14}$$

where $P(\rho)$ and $\mu(\rho)$ are calculated from (9) and (10), respectively.

Equivalently, we can apply the Maxwell equal-area construction to (10), i.e.

$$\int_{\rho_v}^{\bar{\rho}} d\rho[\mu(\rho) - \bar{\mu}] = \int_{\bar{\rho}}^{\rho_L} d\rho[\mu(\rho) - \bar{\mu}] \tag{15}$$

where $\rho_v < \bar{\rho} < \rho_L$ and $\mu(\bar{\rho}) = \bar{\mu}$.

A typical $\mu(\rho)$ against ρ family of curves at different isotherms, together with a schematic diagram for the Maxwell equal-area construction, is shown in figure 1. The coexistence densities ρ_L and ρ_v at different isotherms are shown in figure 2. Finally, it is straightforward to calculate the surface tension γ by performing the numerical integration

$$\gamma = 2\int_{-\infty}^{\infty} dz f_2(\rho(z))\left(\frac{d\rho(z)}{dz}\right)^2. \tag{6a}$$

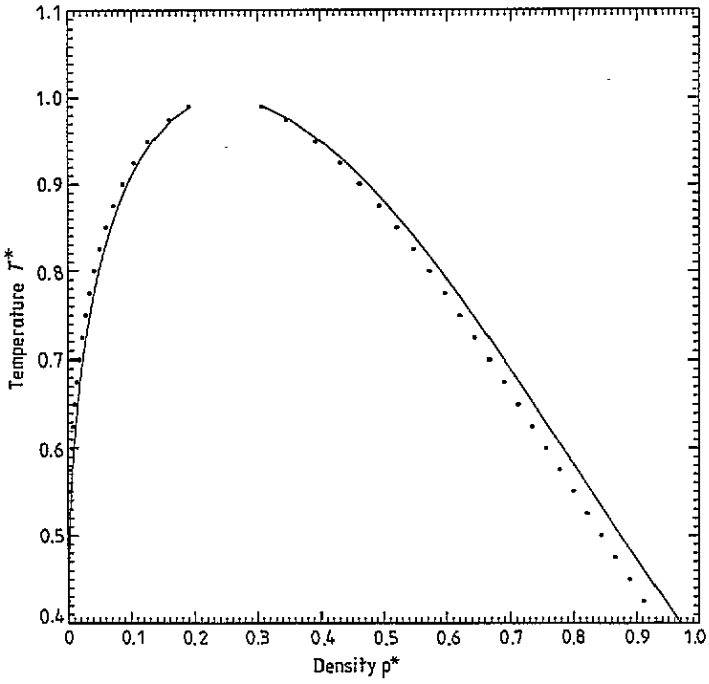

Figure 2. Phase diagram of liquid–vapour coexistence. Points: planar interface; full curves: spherical interface. (Reduced units are used.)

3.2. Spherical interface

We now consider a liquid droplet with a spherically symmetric surface in the presence of a very weak external potential. In this case it is easier to take the origin at the drop centre. Because of the symmetry, the density varies only radially, and the partial differential equation (5) reduces to an ordinary one in the radial distance r:

$$2f_2(\rho(r))\left(\frac{\mathrm{d}^2\rho(r)}{\mathrm{d}r^2}+\frac{2}{r}\frac{\mathrm{d}\rho(r)}{\mathrm{d}r}\right)+f_2^1(\rho(r))\left(\frac{\mathrm{d}\rho(r)}{\mathrm{d}r}\right)^2-f_0^1(\rho(r))+\bar{\mu}=0 \tag{5b}$$

and for the surface tension, (6) becomes

$$\gamma=2\int_0^\infty \mathrm{d}r f_2(\rho(r))\left(\frac{\mathrm{d}\rho(r)}{\mathrm{d}r}\right)^2. \tag{6b}$$

Here the necessary boundary conditions for (5b) are

$$\rho(0)=\rho_L \qquad \rho(\infty)=\rho_v \tag{16}$$

where ρ_L and ρ_v are self-consistently determined from

$$P(\rho_L)-P(\rho_v)=2\int_0^\infty \mathrm{d}r\left(\frac{2f_2(\rho(v))(\mathrm{d}\rho(r)/\mathrm{d}r)^2}{r}\right) \tag{17}$$

and

$$\mu(\rho_L)=\mu(\rho_v)=\bar{\mu}. \tag{18}$$

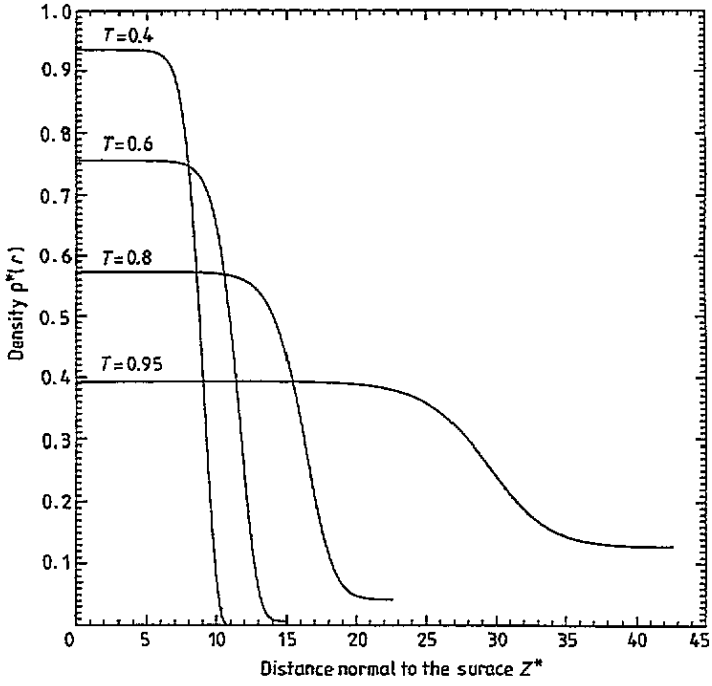

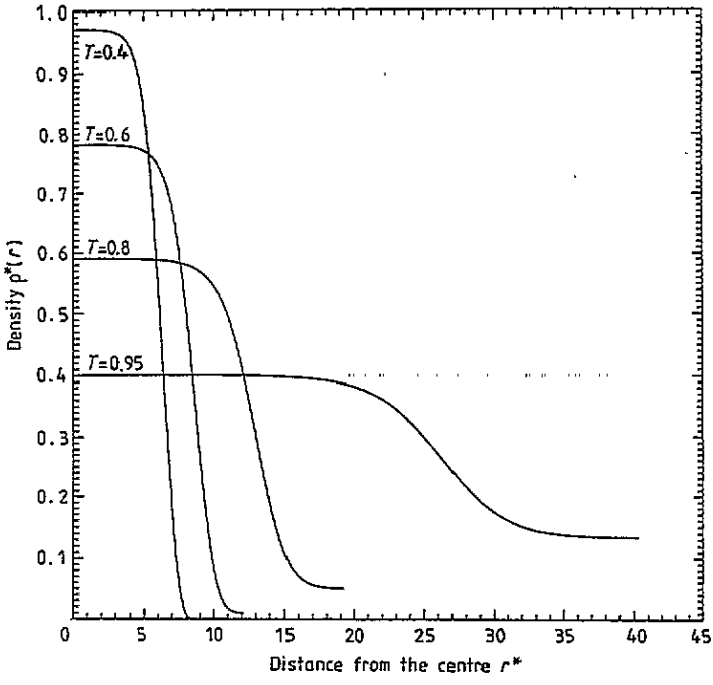

Figure 3. Density profile of the liquid–vapour interface (in reduced units) at different isotherms. (*a*) Planar interface. (*b*) Spherical interface.

Equation (17) is the gradient expansion expression for the generalized Young–Laplace equation which ensures the condition of mechanical equilibrium [2]. Thermodynamically, a liquid drop of critical nucleation radius R is stable when the surface tension γ is related to the pressure difference between the bulk liquid and vapour through the familiar Young–Laplace relation [17]

$$P(\rho_L) - P(\rho_v) = \frac{2\gamma}{R}. \tag{19}$$

The number of molecules in each drop is, generally, defined as

$$N = \int_0^R \mathrm{d}^3 r \rho(r). \tag{20}$$

We have carried out two different sets of calculations for solving (5b). The first set is related to an open system of constrained volume, temperature and chemical potential while the number of molecules is not kept constant. In this system, the boundary conditions given by (16) and the condition of uniform chemical potential expressed by (18) hold and are known in advance; the solution of (5b) is then straightforward. The results of these calculations are demonstrated in figures 3–5 and table 1.

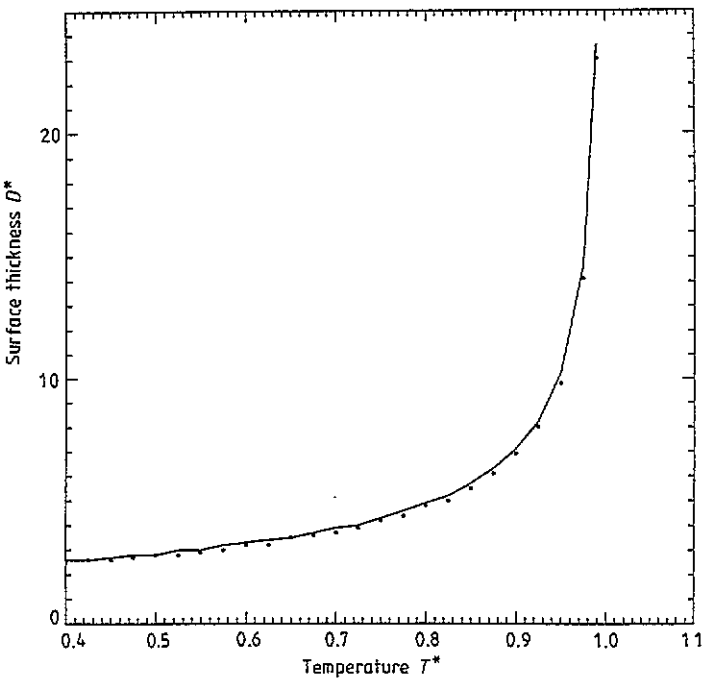

Figure 4. Reduced surface thickness, as calculated from (22), against reduced temperature. Points: planar interface; full curves: spherical interface.

The second set of calculations is for a closed system in which the number of molecules is fixed while the Lagrange multiplier $\overline{\mu}$ is taken to be the chemical potential of a uniform vapour, because we are interested in a liquid drop at equilibrium with a uniform vapour

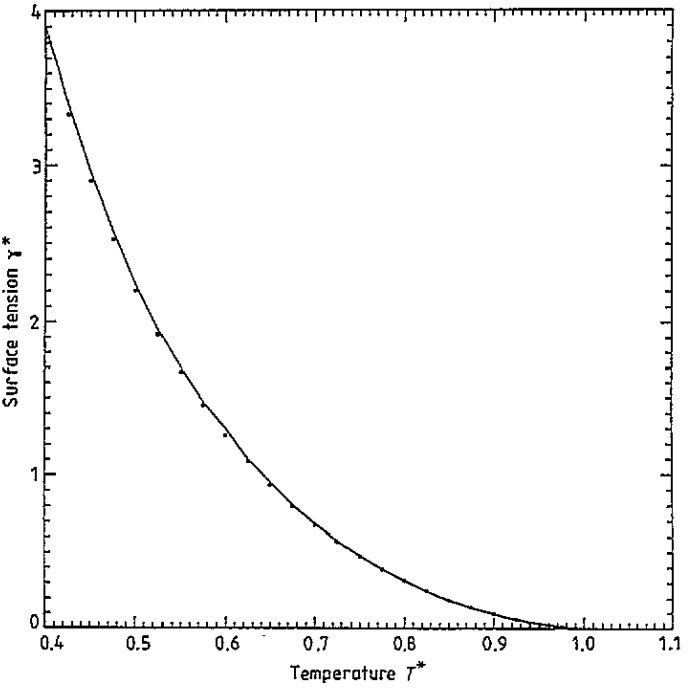

Figure 5. Reduced surface tension against reduced temperature. Points: planar interface; full curves: spherical interface.

phase rather than in the opposite case of a vapour bubble in equilibrium with a bulk liquid, i.e. (18) is to be replaced by

$$\overline{\mu} = \mu(\rho_v). \tag{21}$$

To be more specific, in order to fix N at different temperatures the following steps are to be followed.

(i) Start with an initial estimate of ρ_L and ρ_v, equations (16) and (21) hold, and then the solution of (5b) gives the equilibrium density profile $\rho(r)$.

(ii) Substitute $\rho(r)$ into (3), (6b), (19) and (20) to calculate $\Omega[\rho(r)]$, γ, R and N, respectively.

(iii) Keep ρ_v fixed and change ρ_L to generate a set of solutions $\rho(r)$ and the corresponding $\Omega[\rho(r)]$, R and N. Monitor $\Omega[\rho(r)]$ as a function of R. The maximum of $\Omega[\rho(r)]$ gives the radius of the thermodynamically stable drop.

(iv) Change ρ_v and repeat steps (i)–(iii) to fix the number of molecules N in such a thermodynamically stable drop.

The results of the second set of calculations are shown in table 2 and figure 6.

Since (5a) and (5b) are complicated non-linear differential equations, it is not feasible to get analytical solutions. Numerically, the solution is based on a mixed method of an initial-value problem 'four-steps' Runge–Kutta method [18] and the shooting technique.

4. Results and discussion

Throughout the whole set of results, we have carried out our calculations in reduced units. Thus, for density: $\rho^* = \rho\sigma^3$; for temperature: $T^* = k_B T/\epsilon$; for pressure: $p^* = p\sigma^3/\epsilon$;

Table 1. Comparison of bulk and surface properties for the planar (P) and Spherical (S) interfaces. $\Delta P = P(\rho_L) - P(\rho_v)$ (all quantities are in reduced units).

T	ΔP	ρ_L	ρ_v	N	F/N	γ	D	R	
0.40	0.0	0.9360	0.0001	——	−6.612	3.832	2.50	——	P
	1.2665	0.9703	0.0004	774	−6.521	3.906	2.60	6.08	S
0.50	0.0	0.8438	0.0013	——	−5.874	2.200	2.80	——	P
	0.6212	0.8745	0.0027	1145	−5.698	2.238	2.80	7.11	S
0.60	0.0	0.7556	0.0061	——	−5.445	1.257	3.20	——	P
	0.3007	0.7824	0.0095	1723	−5.317	1.297	3.30	8.38	S
0.70	0.0	0.6670	0.0181	——	−5.382	0.677	3.70	——	P
	0.1341	0.6896	0.0237	2596	−5.214	0.685	3.90	10.08	S
0.80	0.0	0.5730	0.0418	——	−5.535	0.314	4.80	——	P
	0.0489	0.5908	0.0490	4474	−5.372	0.313	4.90	12.73	S
0.90	0.0	0.4635	0.0868	——	−6.201	0.096	6.90	——	P
	0.0103	0.4756	0.0942	10 935	−6.039	0.095	7.10	18.37	S
0.95	0.0	0.3932	0.1269	——	−7.059	0.032	9.80	——	P
	0.0024	0.4014	0.1332	26 649	−6.906	0.031	10.20	26.03	S
0.99	0.0	0.3064	0.1903	——	−8.985	0.002	23.00	——	P
	0.0001	0.3098	0.1937	265 428	−8.876	0.002	23.60	58.81	S

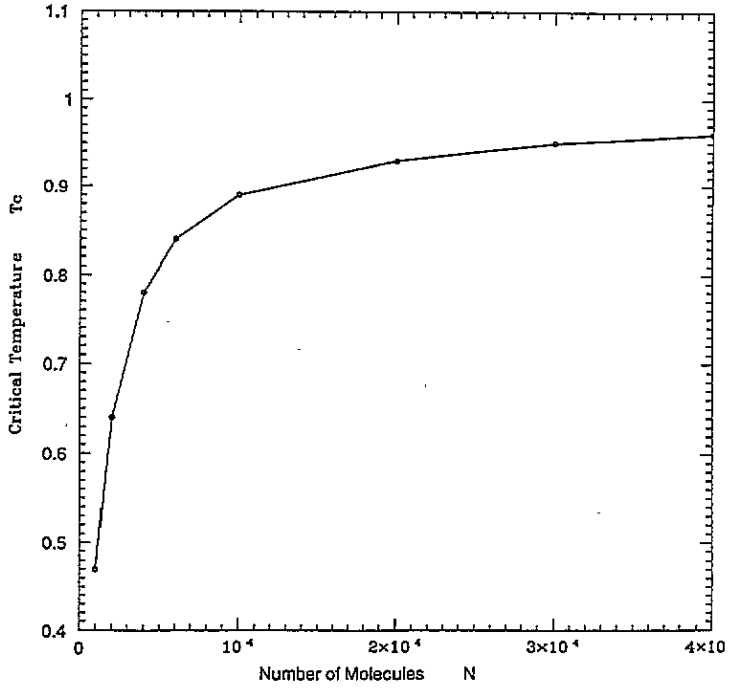

Figure 6. The reduced critical temperature for microscopic liquid droplets.

for chemical potential: $\mu^* = \mu/\epsilon$; for distances and diameters: $r^* = r/\sigma$; and for surface tension: $\gamma^* = \gamma\sigma^2/\epsilon$.

In figures 3(*a*) and 3(*b*) we plot the density profiles $\rho(r)$ as obtained from the numerical solution of (5*a*) and (5*b*), respectively. In figure 3(*a*) the zero of z is located in the bulk liquid, while in figure 3(*b*) the zero of r is taken to be at the drop centre. It is obvious that the profile is a monotonically decreasing function with increasing r and approaches the vapour density at a quite large r. Furthermore, the width of the transition region of $\rho(r)$ is much sharper at low temperatures, while it becomes infinitely large at the critical temperature. For comparison, the profile of the spherical interface decreases more sharply than that of the planar interface at the same temperature, which can be related to the curvature effects of the interface.

For the definition of the surface thickness, D, (the width of the transition region of $\rho(r)$ is conventional), we follow the definition given in [1] and used by several authors [4–6]. This is known as the 10–90 thickness, which is defined as

$$D = r(\bar{\rho}_v) - r(\bar{\rho}_L) \tag{22}$$

where

$$\bar{\rho}_v = 0.9\rho_v - 0.1\rho_L \qquad \bar{\rho}_L = 0.9\rho_L - 0.1\rho_v.$$

In figure 4, we compare the surface thickness of a spherical interface with that of a planar interface calculated at the same temperature. In figure 5, we present our results for the surface tension for both the planar and spherical interfaces as calculated from (6a) and (6b), respectively. The differences at all temperatures are very small because all the droplets are large ($R > 6\sigma$), and therefore their surface tension approaches that of the planar interface. It is remarkable that the surface tension approaches zero at the critical temperature, which agrees fairly well with the criticality of the liquid–vapour transition.

For comparison, we also present in table 1 all available results for the bulk and surface properties of both types of interfaces; ΔP denotes the pressure difference, $P(\rho_L) - P(\rho_v)$, which is non-zero in the case of a spherical interface according to the Young–Laplace [17] relation (19). Also, we present the free energy per particle, F/N, as defined as the sum of the free energy of a particle in the bulk liquid plus that for a particle at the equimolar surface [1].

Finally, in table 2, we present the surface and bulk properties for several liquid droplets each of a fixed number of molecules, N, and show the effect of temperature on the drop radius R. As is well known [19], this Young Laplace radius R provides the critical nucleation size of a liquid drop at a given temperature. It is quite difficult, numerically, to fix the N at different temperatures because of the numerical integration in (20). The uncertainty in N is found to be within 1%, which is not too bad, particularly for large droplets. From table 2 we make the following observations.

(i) For each droplet there is a critical temperature and pressure (marked by '+') at which the droplet evaporates.

(ii) For a particular droplet, with increasing temperature the surface tension decreases while the surface thickness increases. This behaviour is exactly the same as in the case of a liquid–vapour interface of infinite size (a planar interface).

(iii) The surface tension at the critical temperature decreases with increasing drop size.

(iv) The free energy per particle can be considered as an indicator of the stability of each droplet against size increase. It is clear that the droplets with a larger number of molecules are more stable.

Table 2. The bulk and surface properties for several droplets with a number of molecules in the range 1000–40 000. $P_L = P(\rho_L)$. The critical temperatures and pressures are indicated by '+'. (All quantities are in reduced units.)

N	T	P_L	ρ_L	F/N	γ	D	R
1000	0.40	1.168	0.968	−6.322	3.913	2.60	6.60
	0.45	0.868	0.921	−5.968	2.953	2.70	6.70
	0.47	+0.768	+0.902	−5.815	2.643	2.80	6.79
2000	0.40	0.940	0.962	−6.387	3.921	2.50	8.23
	0.50	0.519	0.870	−5.741	2.245	2.90	8.54
	0.60	0.283	0.781	−5.339	1.275	3.20	8.90
	0.64	+0.219	+0.745	−5.238	1.002	3.50	9.04
4000	0.40	0.752	0.957	−6.282	3.916	2.50	10.28
	0.50	0.415	0.865	−5.672	2.245	2.80	10.67
	0.60	0.227	0.776	−5.364	1.278	3.20	11.10
	0.70	0.116	0.686	−5.219	0.684	3.80	11.62
	0.78	+0.061	+0.611	−5.312	0.373	4.60	12.13
6000	0.40	0.657	0.955	−6.518	3.913	2.50	11.76
	0.50	0.364	0.862	−5.692	2.244	2.80	12.17
	0.60	0.199	0.774	−5.353	1.278	3.30	12.66
	0.70	0.102	0.684	−5.247	0.685	3.90	13.28
	0.80	0.044	0.589	−5.383	0.314	4.80	14.02
	0.84	+0.029	+0.547	−5.550	0.211	5.50	14.44
10 000	0.40	0.556	0.952	−6.326	3.906	2.50	13.88
	0.50	0.307	0.860	−5.764	2.241	2.80	14.41
	0.60	0.169	0.771	−5.361	1.278	3.20	14.95
	0.70	0.086	0.682	−5.260	0.685	3.90	15.67
	0.80	0.037	0.587	−5.403	0.315	4.80	16.54
	0.89	+0.012	+0.488	−5.931	0.111	6.70	17.71
20 000	0.40	0.441	0.949	−6.495	3.895	2.50	17.43
	0.50	0.245	0.856	−5.715	2.236	2.80	18.06
	0.60	0.134	0.768	−5.406	1.276	3.20	18.79
	0.70	0.069	0.679	−5.276	0.685	3.80	19.65
	0.80	0.030	0.584	−5.426	0.316	4.80	20.72
	0.90	0.008	0.473	−6.064	0.096	7.00	22.35
	0.93	+0.004	+0.433	−6.480	0.053	8.50	23.09
30 000	0.95	+0.002	+0.401	−6.912	0.031	10.20	27.11
40 000	0.96	+0.001	+0.383	−7.202	0.022	11.40	30.22

For further illustration, we plot in figure 6 the critical temperature T_c as a function of droplet size. It is clear that T_c increases exponentially with N until it reaches asymptotically the critical temperature for the planar interface which corresponds to a droplet of infinite size.

5. Conclusion

To conclude, the following observations are in order.

(i) At this level of description, our model is applicable to all noble gas liquids simply by fitting the potential parameters, σ and ϵ, with their corresponding experimental values (for details, we refer the reader to [5]).

(ii) The gradient expansion together with the simplified random phase approximation give a fairly good account for the liquid–vapour interface and explain, qualitatively, the behaviour of liquid droplets at different temperatures.

(iii) To assess the accuracy of our model we may compare our results for much smaller droplets ($N < 1000$) with the molecular dynamic calculations of Powles and co-workers [13]. We are investigating this at present.

(iv) The satisfactory results obtained in this work for single-component liquids suggest that we may undertake with some degree of confidence the more probing calculations of the surface segregation of liquid-mixture droplets.

Acknowledgment

This work was supported by the International Centre for Theoretical Physics (ICTP, Trieste, Italy) grant no. SMR 428/488. I am grateful to the ICTP for associate membership from January 1990 to December 1995.

References

[1] Rowlinson J S and Widom B 1984 *Molecular Theory of Capillarity* (Oxford: Oxford University Press)
[2] Yang A J M, Fleming P D and Gibbs J H 1976 *J. Chem. Phys.* **64**, 3732
[3] Evans R 1979 *Adv. Phys.* **28** 143
[4] Telo da Gama M M and Evans R *Mol. Phys.* **38** 367
[5] Osman S M and Silbert M 1988 *Phys. Chem. Liquids* **17** 257
[6] Stott M J and Young W H 1981 *Phys. Chem. Liquids* **11** 95
[7] Telo da Gama M M and Evans R 1980 *Mol. Phys.* **41** 1091
[8] Bhatia A B, March N H and Tosi M P 1980 *Phys. Chem. Liquids* **9** 229
[9] Osman S M and Silbert M 1990 *J. Non-Cryst. Solids* **117–118** 646
[10] Hansen J P and Verlet L 1969 *Phys. Rev.* **184** 151
[11] Lee J K, Barker J A and Pound G M 1974 *J. Chem. Phys.* **60** 1976
[12] Chapela G A, Saville G, Thompson S M and Rowlinson J S 1977 *Faraday Trans.* **11 73** 1133
[13] Powles J G, Fowler R F and Evans W A R 1983 *Phys. Lett.* **98A** 421, **96** 289
[14] Bhatia A B and Young W H 1984 *Phys. Chem. Liquids* **14** 47
[15] Thiele E 1963 *J. Chem. Phys.* **39** 474
[16] Wertheim M S 1963 *Phys. Rev. Lett.* **10** 321
[17] Hemingway S J, Henderson J R and Rowlinson J S 1981 *Faraday Symp.* **16** 33
[18] Press W H, Flannery B P, Teukolsky S A and Vetterling W T 1986 *Numerical Recipes* (Cambridge: Cambridge University Press)
[19] Reiss H 1965 *Methods of Thermodynamics* (New York: Blaisdell)